

Microstructure evolution and mechanical properties of $\text{Cu}_{46}\text{Zr}_{47}\text{Al}_7$ bulk metallic glass composite containing CuZr crystallizing phases

F. Jiang^a, D.H. Zhang^a, L.C. Zhang^a, Z.B. Zhang^a, L. He^a, J. Sun^{a,*}, Z.F. Zhang^b

^a State Key Laboratory for Mechanical Behavior of Materials, Xi'an Jiaotong University, Xi'an 710049, People's Republic of China

^b Shenyang National Laboratory for Materials Science, Institute of Metal Research, Chinese Academy of Sciences, 72 Wenhua Road, Shenyang 110016, People's Republic of China

Received 17 December 2006; received in revised form 20 February 2007; accepted 22 February 2007

Abstract

$\text{Cu}_{46}\text{Zr}_{47}\text{Al}_7$ ternary bulk metallic glass (BMG) and its composite containing CuZr crystallizing phases were obtained through water-cooled copper mold casting. There is an obvious microstructure transition of CuZr crystallizing phase due to the decrease in the cooling rate: disperse small dendrites–regular radial dendrites–martensite phase. Under compression, the CuZr crystallizing phases particularly for martensite phase yield first and stimulate the formation of multiple shear bands in the matrix, which enhanced the ductility of the composite. The quasi-static compression fracture surface of the BMG its composites display a mixture of three distinct patterns: vein-like, smooth regions and river-like patterns. The river-like pattern was related with the secondary shear bands or tertiary shear bands and its area fraction on the fracture surface was dependent on the plasticity.

© 2007 Elsevier B.V. All rights reserved.

Keywords: Cu-based metallic glass; Shear bands; Fracture mechanism; Ductility

1. Introduction

Bulk metallic glasses (BMGs) have long been regarded as a potential structural material since their first emergence some 40 years ago. However, monolithic BMGs usually exhibit poor plasticity and no strain hardening ability during room temperature deformation due to highly localized shear bands, which significantly limits the range of possible applications. In order to overcome the limited plastic deformability of BMGs, composites containing ceramic particles [1,2], ductile micrometer-sized particles [3,4], bcc- β dendrites [5,6] or nanostructure-dendrites [7,8] were prepared by ex situ or in situ methods. In these composites, the second phase hinders single shear band to extend critically through the whole sample at the onset of plastic deformation and seeds the initiation of multiple shear bands. Therefore, the plastic strain is distributed more homogeneously in the shear band patterns, which results in high strains to failure of the composites.

Recently, the progress of bulk glass formation in binary Cu–Zr alloys has triggered a lot of interest in rather simple and easy glass-forming systems [9–11]. Moreover, some Cu–Zr-based BMGs such as $\text{Cu}_{50}\text{Zr}_{50}$ [12,13] and $\text{Cu}_{47.5}\text{Zr}_{47.5}\text{Al}_5$ [14] have exhibited large plastic strain with extensive “work-hardening” due to introduce atomic-scale inhomogeneities or nanocrystals. Besides, $\text{Zr}_{48.5}\text{Cu}_{46.5}\text{Al}_5$ BMG composites were developed by in situ precipitation martensite phase and had exhibited good plastic deformability and hardening-like behavior due to the presence of the martensite phase [15]. Comparing with former Zr-, Cu- and Ti-based BMG composites [1–8] and other ductile Pt- and Pd-based BMGs [16,17], the Zr–Cu–Al (or Cu–Zr–Al) ternary alloys have a better combination of strength, ductility and lower production cost. Moreover, as a structure material for BMG and its composites, high yield strength, good ductility and large size are all necessary to meet the requirement. On one hand, BMG composites with large size and good plasticity have so far always been accompanied by poor yield strength due to the high reinforcement content required [18]. For example, $\text{Zr}_{73.5}\text{Nb}_9\text{Cu}_7\text{Ni}_1\text{Al}_{9.5}$ composite with bcc- β dendrites has large size of 10 mm in diameter and high fracture plastic strain of 15.8%. However, its yield strength is as low as 1291 MPa [19]. The as-arc melted Ti-based samples exhibit

* Corresponding author. Fax: +86 2982663453.
E-mail address: junsun@mail.xjtu.edu.cn (J. Sun).

very large plastic strains of 16.5–17.9% with relatively lower yield strengths of 1037–1073 MPa [8]. On the other hand, the BMGs and BMG composites with good ductility and high yield strength previously reported are seldom larger than 3 mm in diameter [3,4,12,14]. Following this, in the previous work [20], $\text{Cu}_{46}\text{Zr}_{47}\text{Al}_7$ BMG and its composites in plate with different thicknesses up to 6 mm were prepared by copper mold casting. Primary crystallizing phases with different microstructures and volume fractions could be obtained under different cooling rate, forming some composites with different mechanical properties. In particular, under compression test, the 2 mm thick monolithic BMG has an yield strength of 1894 MPa and high fracture strength of up to 2250 MPa at plastic strain up to 6% exhibiting apparent “work-hardening” behavior. The 4 mm thick $\text{Cu}_{46}\text{Zr}_{47}\text{Al}_7$ BMG composite containing martensite phase yields at 1733 MPa and finally fails at 1964 MPa with plastic strain of 3.7% [20]. Very recently, a group of Cu–Zr and Ti(Cu,Ni)-base ductile “work-hardenable” BMGs based on “supercooled martensitic alloys” has also been reported [21]. The study on the formation and fracture mechanism of Cu–Zr–Al composite containing CuZr crystallizing phase particular for martensite phase is important to develop BMGs and their composites with a combination of high yield strength, good plasticity, large size and low production cost.

In this paper, the microstructure evolution of CuZr crystallizing phase under different cooling rates and mechanical properties of $\text{Cu}_{46}\text{Zr}_{47}\text{Al}_7$ BMG composite containing CuZr crystallizing phases under compression are systematically investigated.

2. Experimental procedure

The processing and microstructure information about a $\text{Cu}_{46}\text{Zr}_{47}\text{Al}_7$ BMG and its composite containing CuZr crystallizing phases have been reported in the previous paper [20]. Plates with different thicknesses up to 6 mm were prepared by copper mold casting. The 2 mm plate is a fully amorphous structure and the 4 mm plate is composed of CuZr crystallizing phases (33.1% in volume) and a metallic glass matrix (66.9% in volume). The Vickers hardness was measured using a MH-5 Vickers micro-hardness tester with a load of 200 g holding for 15 s. The compressive tests were conducted on a computed-controlled, servo-hydraulic MTS 810 testing machine at a strain rate of $1 \times 10^{-4} \text{ s}^{-1}$ at room temperature. After mechanical tests, all the specimens were observed by a HITACHI S-2700 SEM to reveal deformation and fracture features.

3. Results

3.1. Microstructure evolution of CuZr crystallizing phases

The 2 mm sample has a fully amorphous structure and the 4 mm plate is composed of CuZr crystallizing phases (33.1% in volume) and a metallic glass matrix (66.9% in volume), which has been confirmed by the results of XRD, DSC traces, OM and TEM observations [20]. Fig. 1(a) shows the whole cross section of 4 mm sample. It can be seen that there are some grains with

different size in different regions of the cross section. All the crystallization phases were identified as CuZr phase by XRD. It should be noted that there might be other crystallization phases such as $\text{Cu}_{10}\text{Zr}_7$ and CuZr_2 phases that have not been distinguished by XRD due to the limit of resolution. Detailed optical microscopy observations (see Fig. 1(b–d)) show there are three typical sub-microstructures in grains with different sizes. The first is disperse small dendrites within the small round grains in the edge with sizes less than $150 \mu\text{m}$; the second is a regular radial distribution of dendrites in bigger grains locating mainly between the edge and center, whose sizes are in the range of $150\text{--}380 \mu\text{m}$, and the third is blocky grains with different sizes within the biggest grain mainly in the center part, whose sizes are range from 380 to $600 \mu\text{m}$. The blocky grains display an uneven surface and contain plates with different lengths inside and the plates are self-arranged and align in different subcrystalline regions (see Fig. 1(d)). The surface morphology of the grains reveals that a martensite phase formed during the rapid cooling of the alloy melts [15].

3.2. Mechanical properties

Under compression test at a constant strain rate of $1 \times 10^{-4} \text{ s}^{-1}$, the 2 mm $\text{Cu}_{46}\text{Zr}_{47}\text{Al}_7$ BMG displays an initial elastic deformation behavior with an elastic strain of about 2.0% and has yield strength about 1894 MPa and fracture strength 2250 MPa and exhibits apparent “work-hardening” with significant plastic strain up to 6%. The compressive specimen of 4 mm $\text{Cu}_{46}\text{Zr}_{47}\text{Al}_7$ composite yields at 1733 MPa, followed by an obvious strain hardening up to a plastic strain of 3.7% before fracture. Its compressive fracture stress, σ_C^F , is 1964 MPa [20].

Vickers hardness test was performed to investigate the local mechanical properties of grains with different sizes and sub-microstructure. Fig. 2 shows the Vickers hardness of the grains with different size and sub-microstructure (assuming the size of BMG matrix as zero) in the 4 mm plate. The hardness of BMG matrix is about HV 550 and is slightly lower than that of 2 mm BMG (about HV 580). The hardness decreases with the increase in grain size and that of grains with disperse small dendrites are higher than those of grains with regular radial dendrites and CuZr martensite phase. It can be seen that CuZr martensite phase has the lowest hardness of HV (about HV 370).

3.3. Fracture surface observations

From Fig. 3(a), it can be seen that the compressive specimen of 2 mm BMG fails in a shear mode and its compressive shear fracture angle θ_C is quite close to 45° . Fig. 3(b) shows that the compressive specimens of 4 mm BMG composite also fails in a shear mode and its compressive shear fracture angle θ_C is approximately quite to 43° . Fig. 4(a) shows the surface deformation morphology of the compressed 2 mm BMG by SEM. Many and closely spaced shear bands on side surface should contribute to its large plasticity under compression, which should originate from a unique microstructure correlated with atomic-scale inhomogeneity, leading to an inherent capability of extensive shear band formation, interactions, and multiplication of shear bands

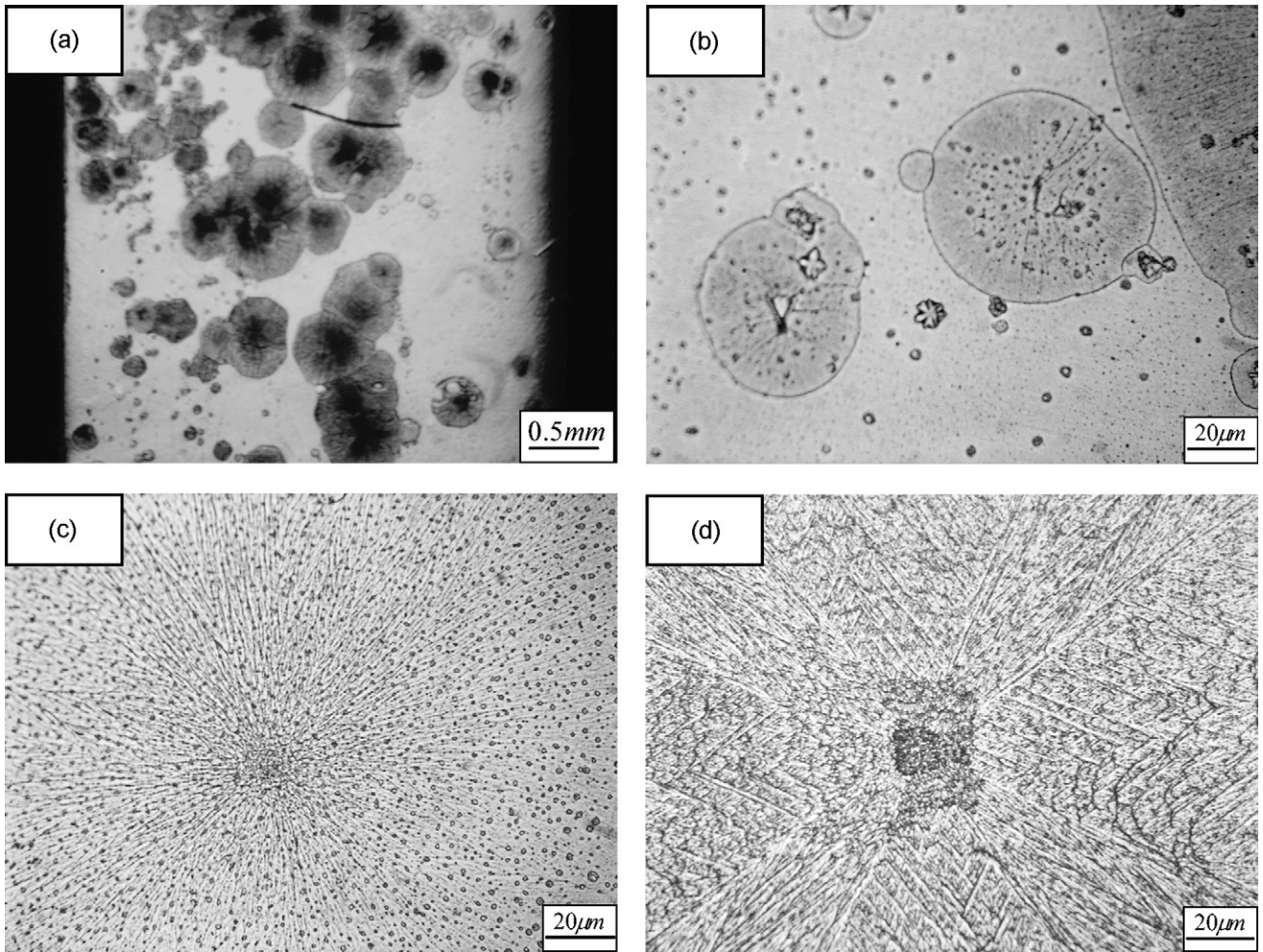


Fig. 1. Optical images of microstructures of the cross-sectional areas of 4 mm $\text{Cu}_{46}\text{Zr}_{44}\text{Al}_7$ alloys for (a) whole cross section, (b) disperse small dendrites, (c) regular radial dendrites and (d) martensite phase.

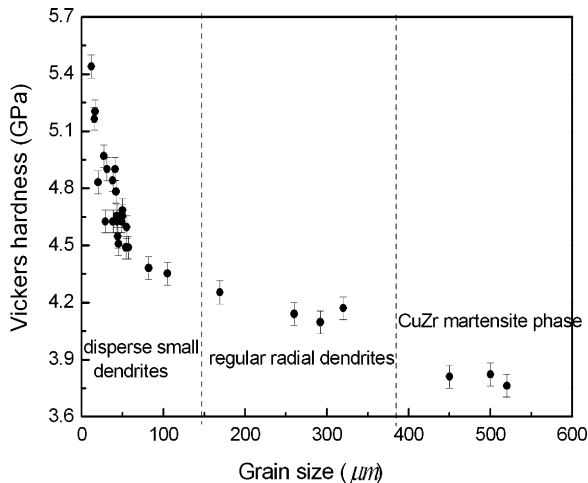


Fig. 2. The Vickers hardness of grains with different sizes and sub-microstructure.

[14]. The observations to the side surface of the compressed 4 mm BMG composite reveal that the CuZr martensite phase deformed firstly due to relative lower yield strength comparing with other grains and BMG matrix, as shown in Fig. 4(b). Dense shear bands were activated as meeting the CuZr crystallizing phases with different grain sizes as shown in Fig. 4(c). The secondary and tertiary shear bands on the deformation surface strongly interact with each other, forming numerous branches. The severe plastic deformation or stress concentration induced cracking of grains with radial dendrites (see Fig. 4(d)). Finally, the compressed specimen fails still in a shear mode as shown in Fig. 4(e). The fracture surface feature of the compressed 2 and 4 mm specimens are exhibited in Fig. 5(a and b). The fracture surfaces are both composed of mixed fracture morphology—(I) vein-like pattern, (II) river-like pattern and (III) intermittent smooth regions. Similar fracture surface feature could also be found in the fracture surfaces of Zr-based BMG composite and Cu-based BMG ($\text{Cu}_{60}\text{Zr}_{30}\text{Ti}_{10}$) [22]. An enlarged micrograph (Fig. 5(c)) presents the localized formation of a river-like pattern. And a typical feature of a combination of veins and some cores under tension of 2 mm $\text{Cu}_{46}\text{Zr}_{47}\text{Al}_7$ BMG is given in Fig. 5(d).

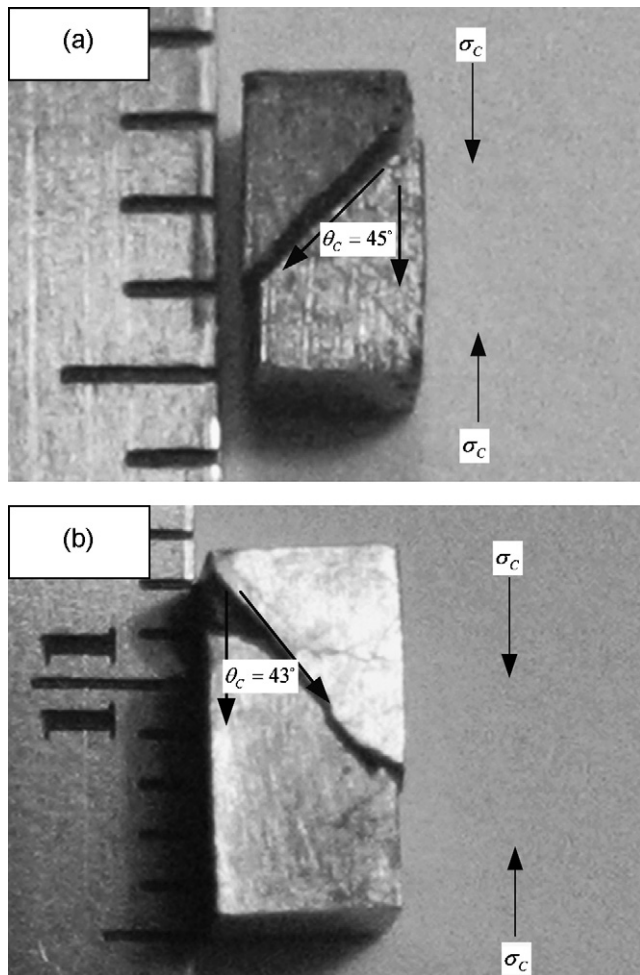


Fig. 3. Fracture feature under compression (a) for 2 mm BMG and (b) for 4 mm BMG composite.

4. Discussions

During the casting, when the cooling rate is higher than the critical cooling rate 370 K/s (estimated from 2 mm plate), $\text{Cu}_{46}\text{Zr}_{47}\text{Al}_7$ fully amorphous glass can be obtained. With the decrease in cooling rate, CuZr crystallizing phase precipitates as the B2 structure (CsCl type bcc based), which exists as line phase above 715°C. Below this temperature, this phase decomposes into the neighbouring stable phases $\text{Cu}_{10}\text{Zr}_7$ and CuZr_2 with an orthorhombic and tetragonal structure, respectively. By rapid cooling to <140 °C the decomposition process is suppressed and the B2 structure transforms into two metastable structures with monoclinic symmetry. These phases have martensitic characteristics and show shape memory behavior [23]. For the 4 mm CuZrAl plate, although the cooling rate is less than the critical cooling rate 370 K/s (estimated from 2 mm plate) and crystallizing phase CuZr precipitates, it is still higher enough to suppress the decomposition process (decomposing into $\text{Cu}_{10}\text{Zr}_7$ and CuZr_2). Part of CuZr crystallizing phases has transformed into martensite phase and the other remained as disperse small dendrites and regular radial dendrites. It is reasonable there is an obvious microstructure transition of crystallizing CuZr from the edge to the center: disperse small dendrites–regular radial

dendrites–martensite phase structure, which emerged and grew bigger with the decrease in cooling rate. With further decrease in the cooling rate, part of CuZr crystallizing phases would decompose into $\text{Cu}_{10}\text{Zr}_7$ and CuZr_2 crystallizing phases.

During the compression, these CuZr crystallizing phases yield first due to their relative lower yield strength. Then dense shear bands were activated as meeting these grains with different grain size. Similarly, a BMG composite with dendritic phase precipitates was investigated using neutron diffraction and self-consistent modeling (SCM) was adopted to ascertain its deformation mechanisms. It was shown that the ductile second phase yielded first upon loading, and this was followed by multiple shear band formation in the matrix, a process which enhanced the ductility of the composite [24]. It could be found that present result has a good agreement with their work. Otherwise, on the edge of 4 mm specimen, many and closely spaced shear bands could be found (Fig. 4(d)). Under loading, the ductility of 4 mm sample is still lower than that of 2 mm thick monolithic BMG because there are grains with various sub-microstructures in the different regions of 4 mm sample in which disperse small dendrites and radial dendrites as “weak spots” reduce the ductility. Recently, a group of Cu–Zr and Ti(Cu,Ni)-base ductile work-hardenable BMGs based on ‘supercooled martensitic alloys’ has been prepared [21]. These composites have a good combination of yield strength, plasticity and large size and are better to meet the requirement as a structure material comparing with their counterpart BMG alloys. However, owing to the different cooling rate from edge to center during casting, the composite obtained generally contains crystallizing phases with different microstructures and mechanical properties. Measurement should be taken to obtain more uniform martensite phases in these casting BMG composites.

In the present work, the fracture surfaces of the 2 mm BMG and 4 mm BMG composites both display a mixture of three distinct patterns: vein-like, smooth regions and river-like patterns as shown in Fig. 5(a and b). However, the previously reported compressed BMGs usually only consist of a quite uniform vein-like structure [25,26]. The vein-like pattern was attributed to local melting within the main shear band induced by the high elastic energy in instantaneous fracture [27,28]. The smooth regions are believed to form when a crack propagates at a high speed after overcoming the trap of a crystalline particle [29]. Those on the fracture surfaces of the Zr-based BMG composite [22] are attributed to the existence of crystals with low volume fraction. The crystalline particle in the present 2 mm BMG and previous $\text{Cu}_{60}\text{Zr}_{30}\text{Ti}_{10}$ [22] should be related with nanocrystallization induced by mechanical deformation. It is reported that quasi-static uniaxial compression imposed on the monolithic Cu–Zr containing amorphous alloys with pronounced plasticity promote nanocrystallization even at room temperature, which was confirmed with high resolution electron microscopy examination [30]. It should be similar to the present Cu–Zr containing $\text{Cu}_{46}\text{Zr}_{47}\text{Al}_7$ BMG and previous $\text{Cu}_{60}\text{Zr}_{30}\text{Ti}_{10}$ [22]. Moreover, the area fraction of smooth regions on the fracture surface should be related with the volume fraction of crystalline particle. It is clear that the area fraction of smooth regions of the 4 mm composites is larger than that of the 2 mm BMG while there is

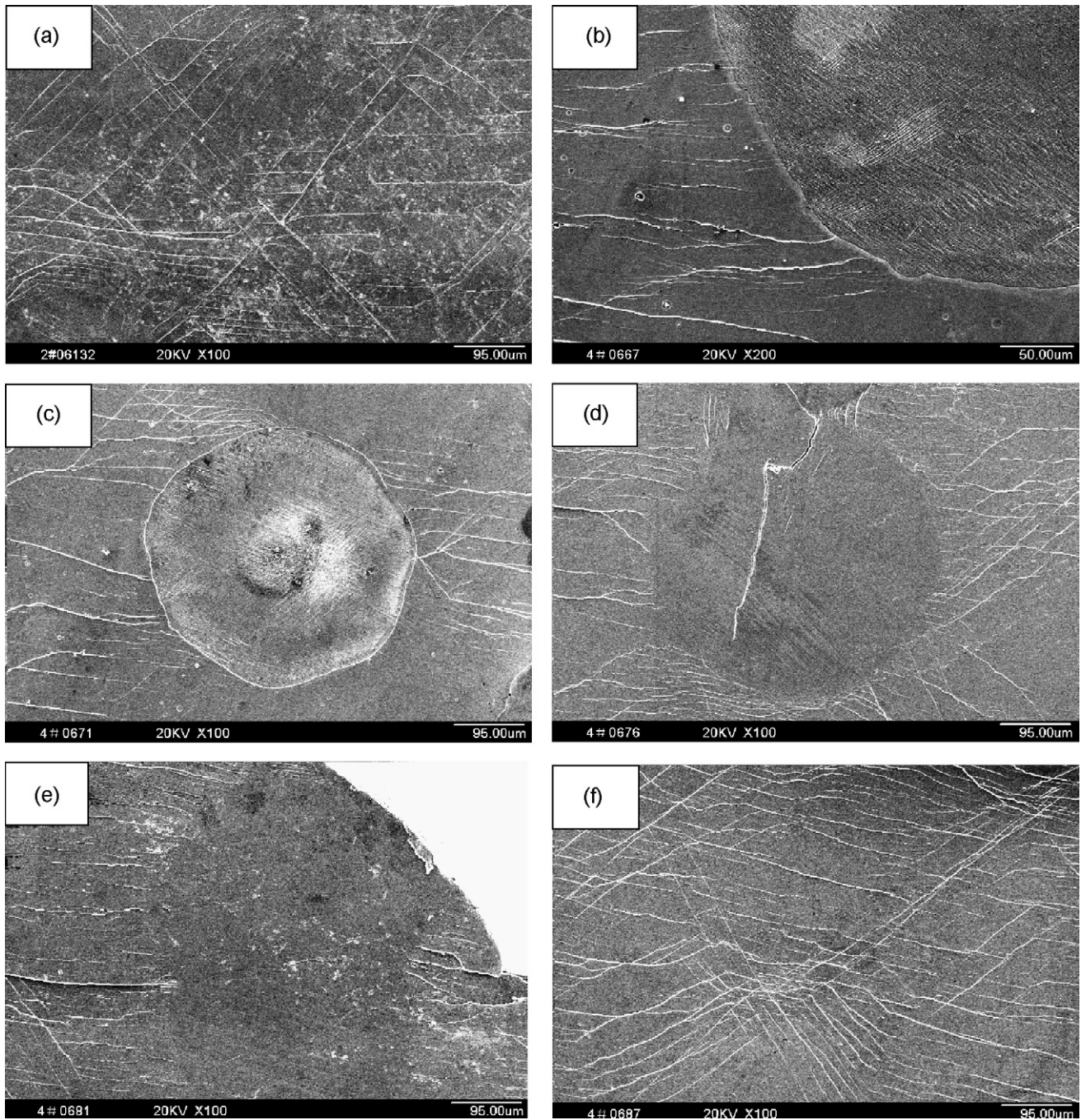


Fig. 4. Surface deformation morphology (a) profuse shear bands on 2 mm BMG side surface, (b–f) deformed CuZr crystallizing phase and multiple shear bands in the matrix of 4 mm BMG composite.

larger volume fraction of CuZr crystallizing phases in the former. Correspondingly, the area fraction of smooth regions of Zr-based BMG [26] is zero due to the absence of crystalline particle.

Besides vein-like pattern and smooth regions, there is river-like pattern on the fracture surface. Kusy et al. [22] has proposed that the river-like pattern formed on transversal steps resembled morphology similar to the one observed on the fracture planes of samples loaded in tension. And it was explained by easy separation along the secondary shear bands at the instability prior to failure due to the significant difference between values of

critical strain accommodation along perpendicular and parallel directions with respect to the shear band planes. The typical feature of a combination of veins and some cores under tension of 2 mm CuZrAl BMG as shown in Fig. 5(d) is similar with these of other many BMGs under tension [25]. It is considered that the radiating cores on the fracture surface are produced by the normal tension stress in the initial stage of fracture, the veins are mainly created by the shear stress during rapid shear propagation [26]. However, it can be seen that there is great difference between this river-like pattern (as shown in Fig. 5(c)) and the typical tension feature. This difference should attribute to the

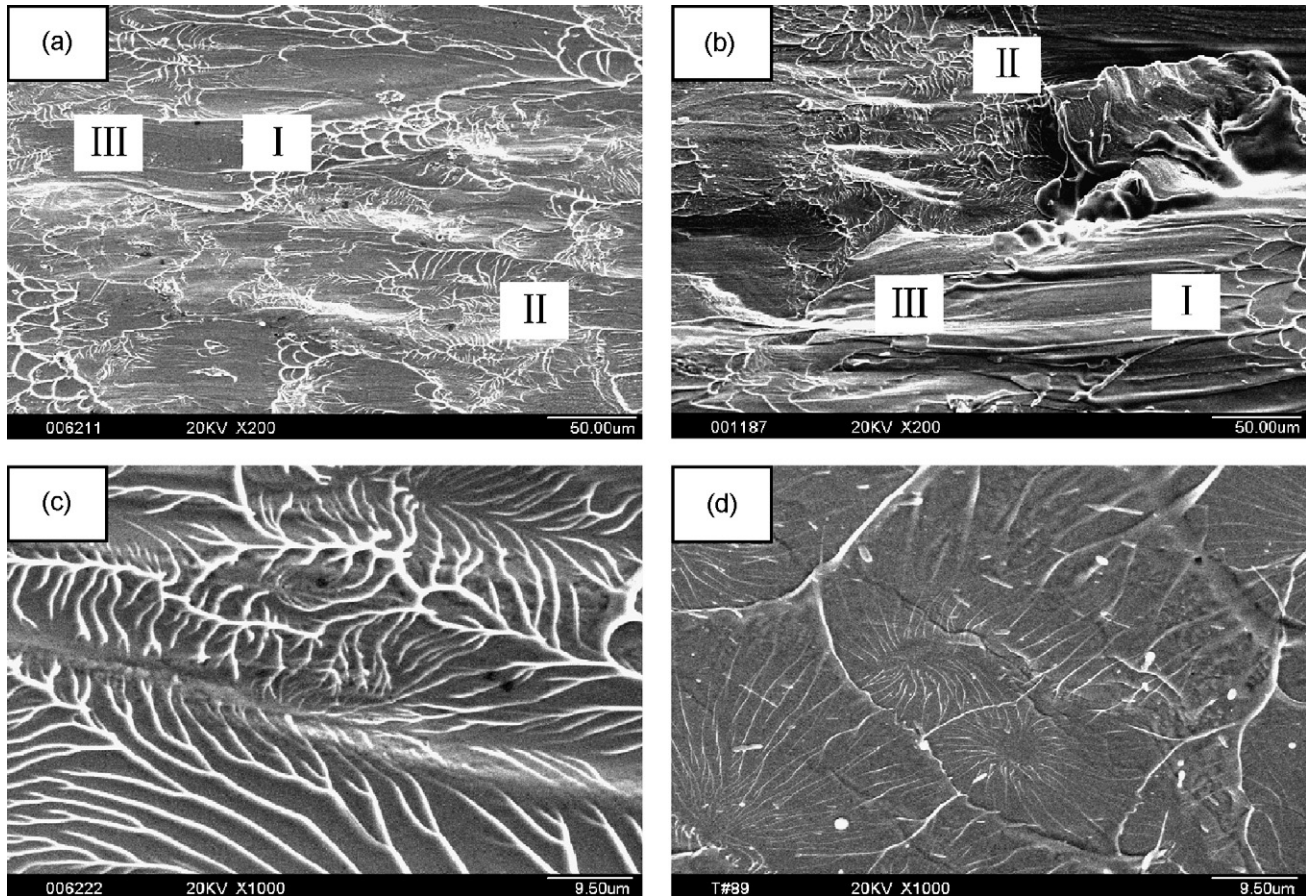


Fig. 5. Fracture surfaces of 2 mm BMG (a) and 4 mm BMG (b) are both composed of mixed fracture morphology—I) vein-like pattern, (II) river-like pattern and (III) intermittent smooth regions. (c) Enlargement of a region with river-like pattern (d) typical feature of a combination of veins and some cores under tension.

stress state. The more ductile the alloy BMGs or BMG composites are, there are more secondary shear bands or tertiary shear bands. It seems that the river-like pattern is related with the secondary shear bands or tertiary shear bands. Accordingly, its area fraction on the fracture surface is dependent on the plasticity. In the BMGs with poor plasticity, fewer secondary shear bands or tertiary shear bands could be formed. And the fracture surface only consists of a quite uniform vein-like structure and fewer river-like patterns were found [26]. With the BMG with enhanced plasticity, the increase of secondary shear bands or tertiary induced the increase in area fraction of river-like pattern [22]. In the present 2 mm Cu–Zr–Al BMG with good plasticity ($\varepsilon_p = 6\%$), the secondary and tertiary shear bands interact strongly each other, forming numerous branches. Large area fraction of vein-like pattern could be found in the fracture surface (see Fig. 5(c)). Similarly, river-like pattern should be found on the fracture surface of ductile BMGs or BMG composites [12–15].

5. Conclusions

(1) There is an obvious microstructure transition of CuZr crystallizing phase due to the different cooling rate during casting: disperse small dendrites–regular radial dendrites–martensite phase.

- (2) Under compression, the CuZr crystallizing phases particularly martensite phase yield first and introduce the formation of multiple shear bands in the matrix, which enhanced the ductility of the composite. However, the plasticity of composite is still lower than that of counterpart BMG alloy whose enhanced compressive plasticity is attributed atomic-scale inhomogenities because disperse small dendrites and radial dendrites as “weak spots” reduce the ductility.
- (3) The quasi-static compression fracture surfaces of BMGs and their composites display a mixture of three different distinct patterns: vein-like, smooth regions and river-like patterns. The river-like pattern was related with the secondary shear bands or tertiary shear bands and its area fraction on the fracture surface is in direct proportion to the plasticity.

Acknowledgements

This work was supported by the National Basic Research Program of China (Grant No. 2004CB619303). The authors also wish to express their special thanks for the support from the National Natural Science Foundation of China Grant Nos. 50501017, 50671076 and 50401019. Z.F.Z. would like to acknowledge financial support from “Hundred of Talents Project” from the Chinese Academy of Sciences and the National

Outstanding Young Investigator Grant of China under Grant No. 50625103. This work was also supported by Program for Changjiang Scholars and Innovative Research Team in University (PCSIRT).

References

- [1] H. Kato, T. Hirano, A. Matsuo, Y. Kawamura, A. Inoue, *Scr. Mater.* 43 (2000) 503–507.
- [2] H. Choi-Yim, R. Busch, U. Koster, W.L. Johnson, *Acta Mater.* 47 (1999) 2455–2462.
- [3] C. Fan, R.T. Ott, T.C. Hufnagel, *Appl. Phys. Lett.* 81 (2002) 1020–1022.
- [4] J.C. Lee, Y.C. Kim, J.P. Ahn, H.S. Kim, S.H. Lee, B.J. Lee, *Acta Mater.* 52 (2004) 1525–1533.
- [5] C.C. Hays, C.P. Kim, W.L. Johnson, *Phys. Rev. Lett.* 84 (2000) 2094–2901.
- [6] Z. Bian, H. Kato, C.L. Qin, W. Zhang, A. Inoue, *Acta Mater.* 53 (2005) 2037–2048.
- [7] G. He, J. Eckert, W. Loser, L. Schultz, *Nat. Mater.* 2 (2003) 33–37.
- [8] G. He, W. Loser, J. Eckert, *Acta Mater.* 51 (2003) 5223–5234.
- [9] D.H. Xu, B. Lohwongwatana, G. Duan, W.L. Johnson, C. Garland, *Acta Mater.* 52 (2004) 2621–2624.
- [10] M.B. Tang, D.Q. Zhao, M.X. Pan, W.H. Wang, *Chin. Phys. Lett.* 21 (2004) 901–903.
- [11] D. Wang, Y. Li, B.B. Sun, M.L. Sui, K. Lu, E. Ma, *Appl. Phys. Lett.* 84 (2004) 4029–4031.
- [12] A. Inoue, W. Zhang, T. Tsurui, A.R. Yavari, A.L. Greer, *Philos. Mag. Lett.* 85 (2005) 221–229.
- [13] Z.W. Zhu, H.F. Zhang, W.S. Sun, B.Z. Ding, Z.Q. Hu, *Scr. Mater.* 54 (2006) 1145–1149.
- [14] J. Das, M.B. Tang, K.B. Kim, R. Theissmann, F. Baier, W.H. Wang, J. Eckert, *Phys. Rev. Lett.* 94 (2005) 205501.
- [15] Y.F. Sun, B.C. Wei, Y.R. Wang, W.H. Li, T.L. Cheung, C.H. Shek, *Appl. Phys. Lett.* 87 (2005) 051905.
- [16] J. Schroers, W.L. Johnson, *Phys. Rev. Lett.* 93 (2004) 255506.
- [17] K.F. Yao, F. Ruan, Y.Q. Yang, N. Chen, *Appl. Phys. Lett.* 88 (2006) 122106.
- [18] H. Choi-Yim, R.D. Conner, F. Szuvecs, W.L. Johnson, *Acta Mater.* 50 (2002) 2737–2745.
- [19] J. Das, W. Loser, U. Kuhn, J. Eckert, S.K. Roy, L. Schultz, *Appl. Phys. Lett.* 82 (2003) 4690–4692.
- [20] F. Jiang, Z.B. Zhang, L. He, J. Sun, H. Zhang, Z.F. Zhang, *J. Mater. Res.* 21 (2006) 2638–2645.
- [21] J. Das, K.B. Kim, W. Xu, B.C. Wei, Z.F. Zhang, W.H. Wang, S. Yi, J. Eckert, *Mater. Trans. JIM* 47 (2006) 2606–2609.
- [22] M. Kusy, U. Kühn, A. Concustell, A. Gebert, J. Das, J. Eckert, L. Schultz, M.D. Baro, *Intermetallics* 14 (2006) 982–986.
- [23] J.W. Seo, D. Schryvers, *Acta Mater.* 46 (1998) 1165–1175.
- [24] B. Clausen, S.Y. Lee, E. Ustundag, C.P. Kim, D.W. Brown, M.A.M. Bourke, *Scr. Mater.* 54 (2006) 343–347.
- [25] Z.F. Zhang, J. Eckert, L. Schultz, *Acta Mater.* 51 (2003) 1167–1179.
- [26] Z.F. Zhang, G. He, J. Eckert, L. Schultz, *Phys. Rev. Lett.* 91 (2003) 045505.
- [27] W.J. Wright, R. Saha, W.D. Nix, *Mater. Trans. JIM* 42 (2001) 642–649.
- [28] C.T. Liu, L. Heatherly, D.S. Easton, C.A. Carmichael, J.H. Schneibel, C.H. Chen, J.L. Wright, M.H. Yoo, J.A. Horton, A. Inoue, *Metall. Mater. Trans. A* 29 (1998) 1811–1820.
- [29] R.D. Conner, H. Choi-Yim, W.L. Johnson, *J. Mater. Res.* 14 (1999) 3292–3297.
- [30] S.W. Lee, M.Y. Huh, E. Fleury, J.C. Lee, *Acta Mater.* 54 (2006) 349–355.